# Remote sensing evaluation of urban heat island and its spatial pattern of the Shanghai Metropolitan Area, China

**Article** *in* Ecological Complexity · January 2009

CITATIONS
9

READS
272

**1 author:**

Hao Zhang
Fudan University
**22** PUBLICATIONS **100** CITATIONS

SEE PROFILE

Ecological Complexity 6 (2009) 413–420

Contents lists available at ScienceDirect

Ecological Complexity

journal homepage: www.elsevier.com/locate/ecocom

# Remote sensing evaluation of urban heat island and its spatial pattern of the Shanghai metropolitan area, China

Juan-juan Li, Xiang-rong Wang, Xin-jun Wang, Wei-chun Ma, Hao Zhang *

*Department of Environmental Science and Engineering, Fudan University, 220 Handan Road, Shanghai 200433, China*

ARTICLE INFO

*Article history:*
Received 23 September 2007
Received in revised form 25 December 2008
Accepted 1 February 2009
Available online 3 March 2009

*Keywords:*
Urban heat island (UHI)
Land surface temperature (LST)
Land use and land cover change (LULC)
Urban sprawl
Shanghai

ABSTRACT

With the aid of an integrated GIS/RS-based approach, methods including spatial autocorrelation, semivariance, and fractal analysis were used to quantitatively characterize the patterns of recent urban heat island (UHI) in the Shanghai metropolitan area during 1997 and 2004. Results show that newly emerging bare lands along the coastal areas and on the remote islands were well vegetated or developed for fishery, and therefore had the significant cooling effect. However, with the rapid expansion of the urbanized and urbaning landscapes, the heating effect of impervious surfaces increased in proportion. Spatial scales showed that the average size of homogeneous patches dominated with the urbanized and urbanizing areas increased remarkably, so did the extent and magnitude of hot spots. Given the growing extent and magnitude of UHI on two dates, dramatic land use and cover change in urban fringes and the major satellite towns significantly exacerbated the UHI effect on regional scale. As a whole, both the extent and magnitude of UHI in Shanghai have undergone a significant increase. Further, the patterns of UHI (as indicated by LSTs) implied the existence of spatial correlation on the small and meso scales. A directional analysis of the Hausdorff–Besicovitch dimension showed that in E–S profile of the city, the spatial dependency of UHI was mainly associated with structural variance. Relatively weak spatial dependency associated with structural variance also existed in the direction of NE–SW. As computed, the structural variation accounted for approximately 50% of the total variation. Therefore, random factors also played the significant role in causing the complexity in patterns of UHI.



## 1. Introduction

Over the past decades population growth and economic expansion have been the primary drivers of land use and land cover change (LULC) worldwide, especially in the developing countries with an increasing desire for prosperous economy. Until recently the urban area accounted for only 2% of the earth surface (Grimm et al., 2000); however, the urbanized and urbanizing landscapes have exerted significant impacts on the local and global ecosystems (Masek et al., 2000). Among tremendous environmental issues associated with human activities, the urban heat island (UHI) effect has been one of the increasing concentrations of urban problems. The UHI phenomenon was commonly referred to as temperature differences between cities and their surrounding rural regions, with higher air temperatures in densely built cities and lower temperatures in surrounding rural regions (Landsberg, 1981).

Previously, measurement of UHI in air temperature was mainly conducted with the data acquired from the weather stations or automobile transects. Recently, measurement of UHI in surface temperature has been used as an alternative on larger scales, by using airborne or satellite remote sensing techniques (Streutker, 2003). Since the 1970s, satellite-derived surface temperature data have been utilized for urban climate analyses on different scales. In addition to thermal data (10.2–12.5 μm) acquired by the Improved TIROS Operational Satellite (ITOS-I), the other thermal data, including Very High Resolution Radiometer (VHRR) data, Heat Capacity Mapping Mission (HCMM) data, Heat Capacity Mapping Mission (HCMM) data (10.2–12.5 μm), Landsat Thematic Mapper (TM) data, Landsat Ehanced Landsat Thematic Mapper plus (ETM+) data, and Moderate Resolution Imaging Spectroadiometer (MODIS) data have been widely utilized (Rao, 1972; Carlson et al., 1977; Price, 1979; Carnahan and Larson, 1990; Hung et al., 2006).

In China, the Yangtze River Basin is one of the most fastly growing regions, with magnitude economy and dense population. Due to rapid influx of population, increasing energy consumption, and resultant changes in land use, uncontrolled urbanization and industrialization have led to an overall environmental degradation in this region. Adverse thermal environment and air pollution at local and regional levels have been one of the major environmental issues. As the economic locomotive and leading mega-city in this region, Shanghai lend itself well to the study of UHI. Historically,

* *Corresponding author*. Tel.: +86 21 55664052; fax: +86 21 65643343.
*E-mail address:* zhokzhok@163.com (H. Zhang).

1476-945X/$ – see front matter © 2009 Elsevier B.V. All rights reserved.
doi:10.1016/j.ecocom.2009.02.002

the firstly recorded UHI phenomenon in Shanghai occurred in the 1950s, and the UHI center was identified at the central part of the old downtown (Zhou and Zhang, 1985). Subsequently, a series of observations revealed that during the 1960–1970s the UHI area expanded gradually and its extent reached nearly 100 $km^2$ in the central urban area. According to a recent study, urbanized and urbanizing areas with observed UHI accounted for 800 $km^2$ (Ding et al., 2002b), which approximately equalled the extent of the central urban area of Shanghai. Having documented profound impacts of urbanization on climate, these studies had focused mostly on UHI effect in the central urban area. However, measurement of change in UHI at regional level will lead to a better understanding of spatial and temporal patterns of UHI, which will meet the very practical needs of urban planning and environmental management, to shape rational urban cluster, relieve adverse effects of human-dominated ecosystem, improve human comfort, etc. Therefore, the purpose of this study is to assess the impact of rapid urban growth on thermal environment by using remote sensing and GIS techniques to measure the change in the surface temperature UHI of Shanghai during 1997–2004.

## 2. Data and methods

### 2.1. Study area

Shanghai is located between latitudes 30°23′N and 31°27′N, and longitudes 120°52′E and 121°45′E (Fig. 1). This area has a northern subtropical monsoon climate, with an average annual temperature about 15 °C. High temperatures average 28 °C in the summer and 4 °C in the winter. The average annual precipitation is approximately 1000–1200 mm, about 60% of rainfall is usually received during May and September.

Shanghai has historically been one of the most important economic centers of China since the early-1900. In the 1920s–1930s, Shanghai was well known as the largest financial center in the Far East (Shen, 1994). This city has experienced a remarkable increase in urban area over the past 50 years. Although the place of this city degraded due to the adverse domestic policies and international factors in 1949–1978, its role as China's most important industrial city attracted millions of workers, and this city was still well known as the biggest city of this country. Fortunately, this city has recently witnessed the unprecedented economic development initialized by the strategy of "opening of Pudong new area to the world" in the 1990s. With the fast growing urban area, the extent of Shanghai metropolitan area sprawled rapidly. At present the Shanghai metropolitan area consists of the following 17 districts or counties: Huangpu, Luwang, Xuhui, Yangpu, Baoshan, Putuo, Pudong, Hongkou, Zhabei, Changning, Jiading, Minhang, Nanhui, Songjiang, Qingpu, Jinshan and Chongming. Currently, Shanghai is the most populous city in China, with approximately 13 million permanent residents in an area of approximately 6400 $km^2$ (Shanghai Municipal Statistics Bureau, 2005).

### 2.2. Detection of LULC

In order to examine the impacts of human activities on regional scale, a land cover classification is necessary for detection of LULC during the rapid urbanization since the 1990s. In this study, the Landsat Thematic Mapper (TM) data acquired on 11 April 1997 and 19 July 2004 were used. The topographical map and land use map (1:100,000) acquired in 1996 and 2003 were used as reference data and for accuracy assessment. The data were resampled using the nearest neighbor algorithm to keep the unchanged original brightness values of pixels, and the RMSE were both found within 1 pixel. The image processing and data manipulation were conducted by using the GEOSTAR® image processing software. According to a pre-determined classification scheme of six categories of land covers present within the study area and their image characteristics, two false true color images were produced by combining bands 5, 4, and 3 of the landsat TM images. The classification scheme of the study area was modified in accordance to the land use classification system by China National Committee of Agricultural Divisions (1984). Herein, the covers consisted of urban or built-up area, farmland, forest, shrub, water (mainly including rivers, creeks, ponds, and lakes), and the bare land. The supervised signature extraction with the maximum likelihood algorithm was employed to perform the classification of the satellite images. Furthermore, for each land category at least 50 samples were randomly selected to check the accuracy of the classified maps, and the KAPPA indices for the 1997 and 2004 maps were 86.7% and 88.3% respectively, which met the recommended value by Lucas et al. (1994). Clearly, these data was available for further study. However, in order to determine the emissivity simply, land use and land cover types were reclassified as the vegetated area (including the forest, farmland, and shrub), water, built-up area, and bare land. Subsequently, land use and land cover patterns for 1997 and 2004 were mapped.

### 2.3. Retrieval of LST

The procedure described by Weng et al. (2004) was adopted for retrieval of land surface temperature (LST). A quadratic model was used to convert the digital number (DN) of landsat TM thermal TIR

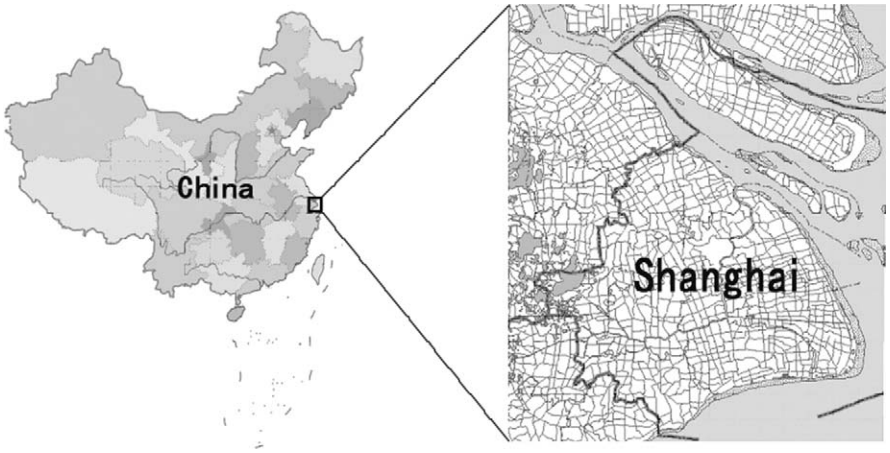


**Fig. 1.** Location of the Shanghai metropolitan area.

band into radiant temperatures (Malaret et al., 1985):

$$T_B = 209.831 + 0.834\mathrm{DN} - 0.00133\mathrm{DN}^2 \quad (1)$$

The temperature values obtained above were referenced to a black body, which is quite different from the properties of real objects. Therefore, correction of spectral emissivity ($\varepsilon$) is a must. Each of the land use types was assigned an emissivity value. It was suggested that the emissivity values should be more detailed considering the nature of land cover types. In this study, the vegetated area, built-up area, bare land, and water bodies were given the values of 0.95, 0.923, 0.92, and 0.9925, respectively (Artis and Carnahan, 1982; Masuda et al., 1988; Nichol, 1994).

Furthermore, the emissivity corrected surface temperature was computed as follows (Artis and Carnahan, 1982):

$$T_s = \frac{T_B}{1 + (\lambda \times T_B/\alpha)\ln\varepsilon} \quad (2)$$

where $T_s$ is the surface radiant temperature in Kelvin (K), $T_B$ the black body temperature in Kelvin (K), $\lambda$ the wavelength of emitted radiance, herein, $\lambda$ = 11.5 μm (Markham and Barker, 1985), $\alpha = hc/K$ ($1.438 \times 10^{-2}$ mK), $h$ = Planck constant ($6.626 \times 10^{-34}$ J s$^{-1}$), and $c$ = velocity of light ($2.998 \times 10^{8}$ m s$^{-1}$), $K$ = Boltzman constant ($1.38 \times 10^{-23}$ J K$^{-1}$), $\varepsilon$ = surface emissivity.

Since the obtained surface radiant temperature is in Kelvin, which is different from the commonly used centigrade. Therefore, the radiant temperature was revised by adding the absolute zero (approximately −273.15 °C) (Xu and Chen, 2004):

$$T_s = \frac{T_B}{1 + (\lambda \times T_B/\alpha)\ln\varepsilon} - 273.15 \quad (3)$$

### 2.4. Detection of spatial heterogeneity of LST

Land properties vary greatly along the rural–urban gradient, so both land use types and LST exhibit spatial dependency. In this study, correlogram and variogram were used to quantify the degree to which samples were spatially autocorrelated and the distance at which this correlation existed. Correlogram is one of the commonly used structure functions to describe spatial structures and dependency. For quantitative variables, Moran's $I$ index is the most often used index to assess the global level of spatial autocorrelation (Cliff and Ord, 1981; Griffith, 1987; Anselin, 1995). Therefore, this study uses correlograms of the Moran's $I$ to quantify the spatial pattern of LST.Moran's $I$ index is defined as

$$I = \frac{n}{\sum_{i=1}^{n}\sum_{j=1}^{n} W_{ij}} \frac{\sum_{i=1}^{n}\sum_{j=1}^{n} W_{ij}(X_i - \bar{X})(X_j - \bar{X})}{\sum_{i=1}^{n}\sum_{j=1}^{n}(X_i - \bar{X})} \quad (4)$$

where $X_i$ and $X_j$ are the values of the observed variable at sites $i$ and $j$, $n$ the total number of sites, $i = 1, 2, \ldots, n$ and $j = 1, 2, \ldots, n$ ($i \neq j$), $\bar{X}$ the mean of all $X_i$ and $X_j$, $W_{ij}$ the weights representing proximity relationships between sites $i$ and $j$; they form together a spatially 0–1 contiguity matrix. Usually, the Moran's $I$ should be standardized to $z$ for judging the positive or negative correlation. In general, the value of Moran's $I$ varies between −1 and +1. Positive autocorrelation in the data produces higher positive values of $I$; negative autocorrelation produces negative values, *vice versa*. A higher positive $I$ implies that the values in neighboring sites tend to cluster together. Whereas a lower negative $I$ implies that high and low values are interspersed. Moreover, the value of $I$ near zero reveals that there is no spatial autocorrelation, indicating the data are randomly distributed (Cliff and Ord, 1981; Legendre and Legendre, 1998).

Variogram, an important and basic function in geostatistics, was used to provide a concise description of the scale and pattern of spatial variability. In practice the semivariogram, indicating the relationship between the semivariance among samples and the lag distance between samples, was often used. Herein, the semivariance $\gamma(h)$ for pixel-based values at distance $h$ apart is defined as

$$\gamma(h) = \frac{\sum_{i=1}^{N(h)} [z(x_i + h) - z(x_i)]^2}{2N(h)} \quad (5)$$

where $\gamma(h)$ is semivariogram of samples with lag distance $h$, $z(x_i)$ and $z(x_i + h)$ the value of variable at sites $x_i$ and $x_i + h$ separately, $N(h)$ the pairs of samples; $h$, usually at regular intervals, meaning the spatial distance of samples (Curran and Atkinson, 1998).

In addition to correlogram and variogram, the fractal dimension was used as another useful tool to measure the spatial pattern of surface temperatures associated with land cover types (Weng et al., 2004). A number of methods were developed for measuring dimensions that are fractional, including the correlation dimension, the box-counting dimension, the information dimension, the capacity dimension, etc. Here we will refer to Hausdorff–Besicovitch dimension, which is the fractal dimension as a function of the slope of a log–log variogram plot (Burrough, 1981).

$$D = 2 - \frac{m}{2} \quad (6)$$

where $D$ is the value of fractal dimension expressed by Hausdorff–Besicovitch statistic, $m$ the slope of a log–log variogram.

To examine the spatial patterns of LSTs on two dates (11 April 1997 and 19 July 2004), transects were drawn across the geographical center of this city in directions of E–W, N–S, NE–SW, and NW–SE. The transects started from the N–S direction and constructed a new transect every 45°, with an offset tolerance of 22.5° in every direction. For spatial autocorrelation, the uniform interval classification method was used in semivariogram analysis. Herein, the lag distance or interval was set as 5 km, and the mean value in distance range as value of semivariance. A range of models is then fitted to the semivariogram by using an unweighted least-squares routine. The spherical model was determined as the best-fit model of semivariogram by using residual sum of squares (RSS). All the spatial analysis processes were performed by using ESRI ArcGIS 9.1 and the DPS 5.12 statistical package (Tang and Feng, 2002). Prior to spatial autocorrelation analysis the normality test was conducted. Fortunately, $P$-value of Kolmogorov–Smirnov and Shapiro–Wilk's $W$-test for the sampled data were much higher than the 0.05 significant level, which can make sure the validity of the dataset.

## 3. Results

### 3.1. Land use pattern in Shanghai

Figs. 2 and 3 show the quite different patterns of LULC over the study period. In 1997, the border between the central urban area and the surrounding towns was very clear, with one center core and sparse towns. Besides, the pattern of emerging bare land was a noteworthiness. Only a small proportion of bare lands existed in the urban fringe due to the rapid development, whereas most of the bare lands existed along the coast and in the remote islands. Based on historical data and field survey, it can be judged that the bare lands existing along the coast and in the remote islands were artificially made for the purpose of docking and shipping facilities, farm lands, and embankments. In contrast, in 2004 with the rapid urban sprawl, both the central urban area and the surrounding towns remarkably increased in their extents. A more closer linkage between the central urban area and the suburban areas was established via the perfect highway systems, including the outer cycle highway and two inter-province highways: Hu-Ning (Shanghai-Nanjing)

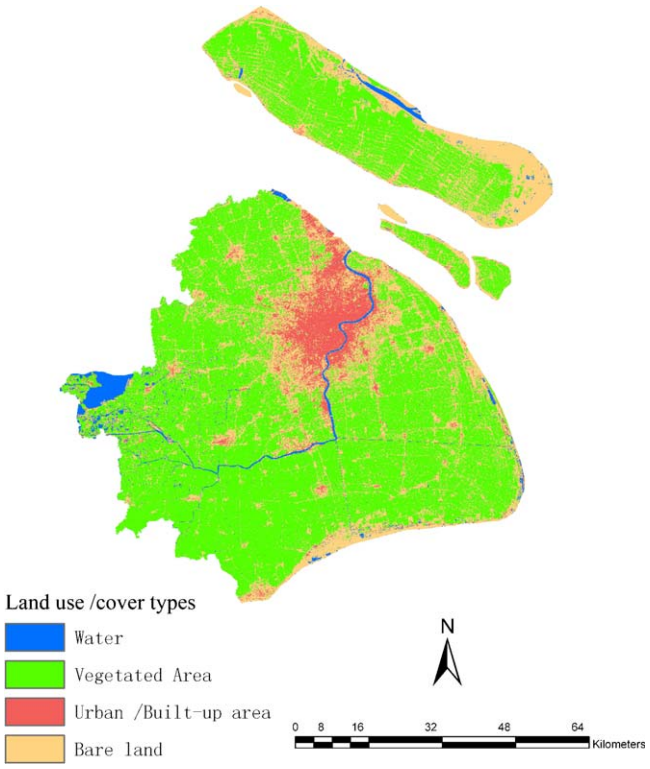


**Fig. 2.** LULC maps of Shanghai on 11 April 1997.

highway and Hu-Hang (Shanghai-Hangzhou) highway. Spatially, the central urban area extended outwards in all directions, especially in S–N, SW–NE, and NW–SE, where the newly emerging satellite towns (including Jiading, Anting, Songjiang, Qingpu, Xinzhuang, Luodian, Baoshan, Gaoqiao, Jinqiao, Luchaogang, etc.) and the major industrial parks were well developed.

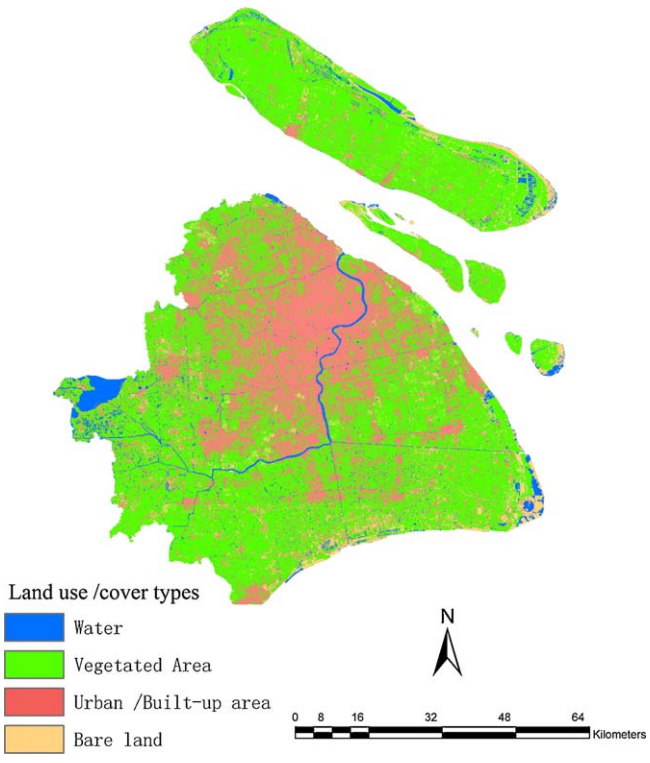


**Fig. 3.** LULC maps of Shanghai on 19 July 2004.

### 3.2. Spatial and temporal distribution pattern of UHI

Summarized characters of LSTs on two dates are shown in Table 1. Herein, the retrieved land surface temperatures dated on 11 April 1997 and 19 July 2004 were written in the concise form of $LST_{1997}$ and $LST_{2004}$. The 1997 image was taken in the mid-Spring, land surface temperatures ranged from 7.3 °C to 37.7 °C, with an average of 22.4 °C. The 2004 image was taken in the mid-Summer, land surface temperatures ranged from 19.67 °C to 43.59 °C, with an average of 31.2 °C. Standard deviation of $LST_{1997}$ was lower than that of $LST_{2004}$, indicating slightly higher variation of $LST_{2004}$.

Figs. 4 and 5 show the increasing extent of UHI over the study period. In 1997, the areas with higher surface radiant temperature were mainly located in the central urban area and the major towns, with a typical strip-shaped associated with the traffic road systems. Within the urban central area, numerous sub-centers of UHI with higher surface radiant temperature were mainly located in the old and recently developed downtowns at middle section of the Huangpu River. Wusongkou, an area characterized with intensive traditional industries at the downstream of the Huangpu River, was also a key contributor to UHI phenomenon. At regional level, the bare lands had higher surface radiant temperatures, especially at the urban fringe and along the coastal areas. Not surprisingly, the water bodies had the lowest surface radiant temperatures, followed by the vegetated areas.

Compared to the UHI map of Shanghai in 1997, the extent of UHI in 2004 increased significantly. With the growing central urban area, the extent of UHI dramatically expanded from the inner cycle highway to the outer one, linking the suburban areas and the substantially growing satellite towns, which were characterized with small and obvious sub-centers with higher surface radiant temperatures. On the other hand, at the south and southeastern parts of Shanghai, which covers most of the rural areas of Jinshan, Fengxian and Nanhui districts, the detected hot spots in 1997 remarkably decreased or disappeared in 2004, except a new hot spot appeared at the recently emerging Linggang new town at the northeastern corner. Similarly, remarkably decrease in strip-shaped hot spot was observed at the east corner of Chongming island and the small islands at the estuary of the Yangtze River.

### 3.3. Relationship between land use/cover types and UHI patterns

Difference in UHI patterns is associated with many factors, including changes in land use, urban surface geometry, seasonal variation, climatic and meteorological condition, etc. (Roth et al., 1989; Voogt and Oke, 1998; Weng et al., 2004; Xu and Chen, 2004). Due to the limited remotely sensed data, it is somewhat difficult to explicate the influences of these factors on UHI patterns. Therefore, relationship between land use/cover types and UHI patterns will be focused on.

Masking land use/cover maps in 1997 and 2004 over the corresponding LST maps, a similar variation trend was found, though the extent of UHI in 1997 was somewhat different from that of land use on the same date. It was found that the built-up

**Table 1**
Descriptive statistics of land surface temperature in 1997 ($LST_{1997}$) and 2004 ($LST_{2004}$).

| Statistics | $LST_{1997}$ | $LST_{2004}$ |
|---|---|---|
| Minimum | 7.3 | 19.67 |
| Maximum | 37.7 | 43.59 |
| Mean | 22.4 | 31.2 |
| Standard deviation | 2.8 | 2.89 |
| Skewness | 0.17 | 0.17 |
| Kurtosis | 0.6 | −0.12 |

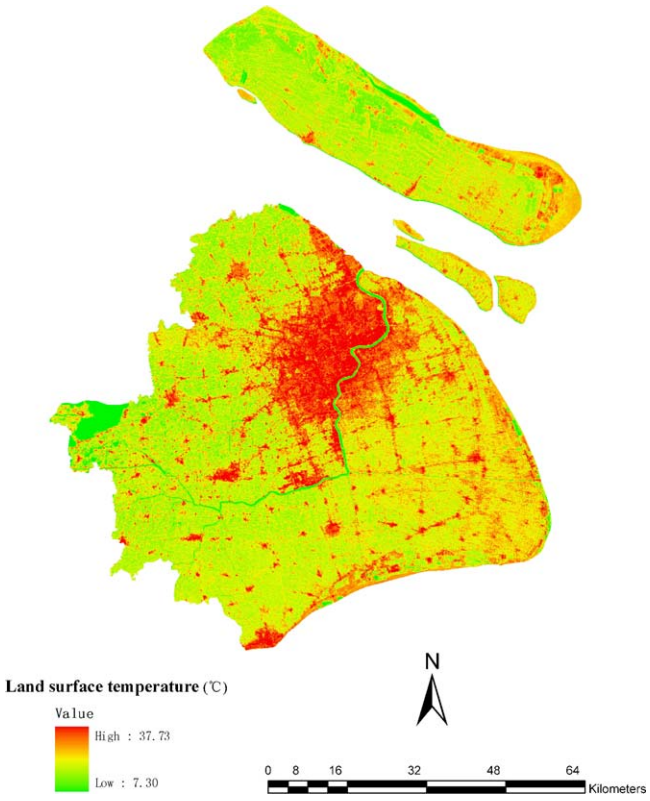


**Fig. 4.** Spatial pattern of $LST_{1997}$ in Shanghai.

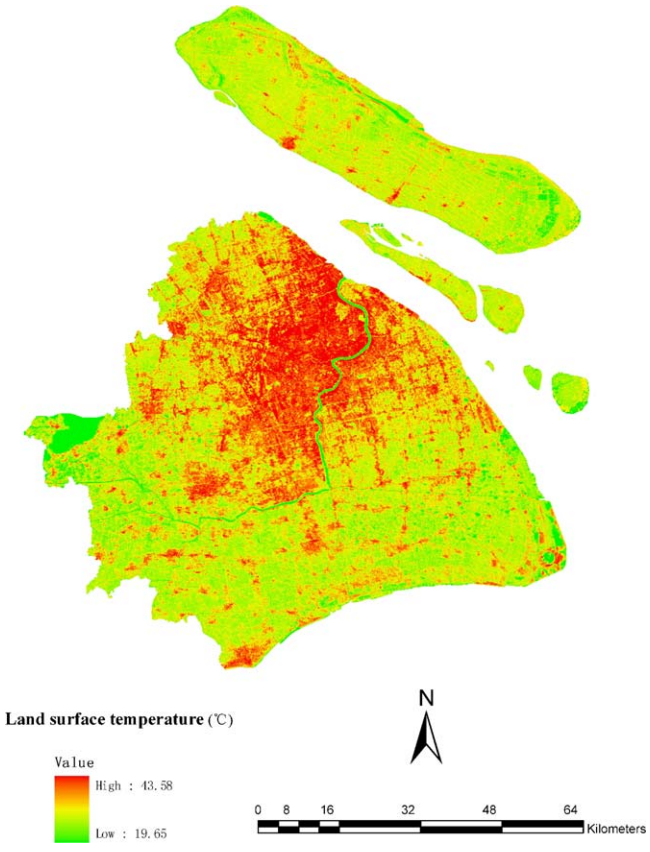


**Fig. 5.** Spatial pattern of $LST_{2004}$ in Shanghai.

area increased by 23.87% in 2004. Spatially, dramatic land use and cover change driven by urbanization occurred in the following areas: (1) the urban fringes along the outer cycle highway, such as Wusongkou industrial park, Huajing town, Hongqiao town and Caohejing town, etc.; (2) the major satellite towns with intensive industrial parks or economic development zones, such as Anting, Jiading and the other towns mentioned in Section 3.1; (3) coastal towns developed for the airport and harbor, such as Jichang town near Pudong international airport and Lingang new town, an access to the Yangshan harbor. These may help to explain the spatial and temporal patterns of UHI. As shown in Figs. 2 and 3, numerous newly hot spots emerged and expanded along the highways linking the central urban area and the surrounding satellite towns, especially in the directions of E–W, S–N, SW–NE and NW–SE. More noticeable low spots, though small, were detected in the central urban area, this may partly attribute to well-preserved Jiangwan wetland, Gongqin forest park, Shanghai plant garden, Xijiao park and massive newly emerging patches of green spaces. In addition, there were only smaller and sparse hot spots in the western part of Shanghai, where farmlands and water prevailed due to the demand for protecting the catchment of Dianshan lake and upstream of the Huangpu River. For the southern and southeastern parts of rural areas and Chongmin island, where bare lands were changed into ponds, farmlands, and shelter belt, which, in turn, presented lower surface radiant temperatures.

Quantitatively, Table 2 shows the average land surface temperatures of each land cover type. Clearly, on two dates the built-up area presented the highest land surface temperature, followed by bare land. The vegetated area and water took third and fourth places, respectively. In comparison to the lower LSTs of each land cover type in 1997, increasing LSTs of each land cover type in 2004 were detected; indicating seasonal variation should not be neglected when exploring the spatial and temporal pattern of UHI indicated by LSTs. However, differences in land surface temperatures reflected the impacts of land use changes on the thermal environment. Given the growing extent and magnitude of UHI on two dates, dramatic land use and cover changes in urban fringes and the major satellite towns exacerbated the regional UHI effect.

### 3.4. Spatial characteristics of the UHI patterns

#### 3.4.1. Spatial autocorrelation analysis of UHI patterns

Figs. 6 and 7 show the Moran's *I* of LSTs on two dates versus the lag distance. As can be seen from the curves, positive and negative spatial autocorrelation of LSTs exist over all distance scales. For $LST_{1997}$, Moran's *I* decreased faster before the critical scale (about 29.5 km), indicating spatial pattern of homogeneous patches on small scales. A negative correlation appeared between 29.5 km and 78 km, indicating spatial pattern of heterogeneous patches on meso scales. The fast increase of Moran's *I* with growing distance was observed at the scale more than 78 km, indicating the distance of homogeneous patches on large scales. For $LST_{2004}$, Moran's *I* decreased faster before the critical scale (about 32 km). A negative correlation appeared between 32 km and 75 km. The increase of Moran's *I* with growing distance was observed at the scale more than 75 km.

**Table 2**
Average LST (mean ± S.D.) associated with land covers.

| Land use/cover types | $LST_{1997}$ | $LST_{2004}$ |
|---|---|---|
| Built-up area | 27.13 ± 3.04 | 34.02 ± 2.45 |
| Bare land | 24.08 ± 3.90 | 33.41 ± 2.30 |
| Vegetated area | 22.34 ± 2.81 | 31.63 ± 2.84 |
| Water | 18.03 ± 2.16 | 27.13 ± 2.06 |

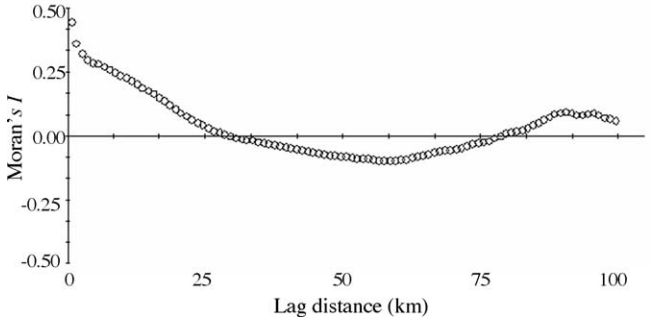


**Fig. 6.** Isotropic spatial correlogram of $LST_{1997}$.

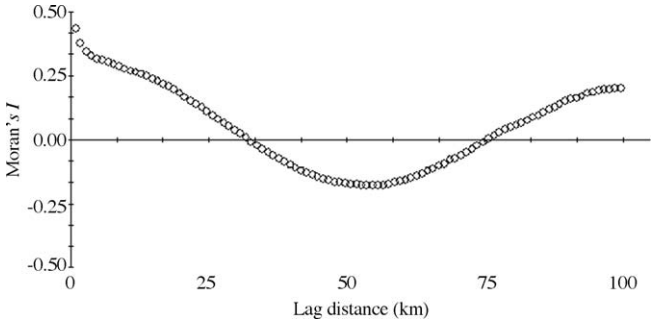


**Fig. 7.** Isotropic spatial correlogram of $LST_{2004}$.

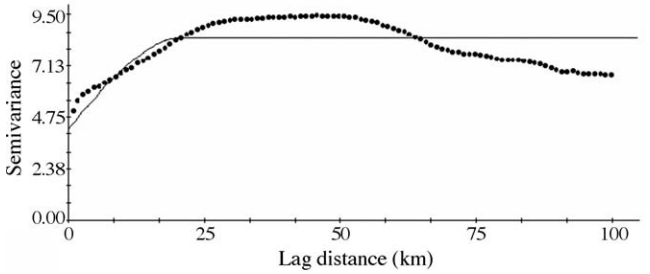


**Fig. 8.** Isotropic semivariograms of $LST_{1997}$.

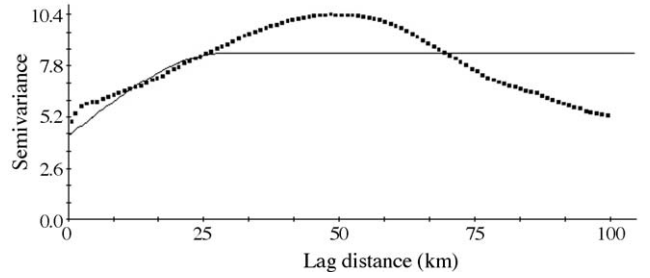


**Fig. 9.** Isotropic semivariograms of $LST_{2004}$.

Generally spoken, the first positive correlation distance in correlograms indicates the mean size of homogeneous patches. Whereas the negative correlation distance indicates the mean distance of heterogeneous patches. The second positive correlation appearing in correlograms indicates the expected distance between homogeneous patches (Zhang et al., 1998). In this study, a rapid change in land use occurred in the central urban area and surrounding satellite towns over the study period. The average size of homogeneous patches dominated with the urbanized and urbanizing areas increased remarkably, so did the extent and magnitude of hot spots. Spatially, with reference to Figs. 3 and 4, decrease in distance between heterogeneous patches and the homogeneous patches can be well interpreted.

*3.4.2. Semivariance analysis of UHI patterns*

Significant spherical models were constructed for $LST_{1997}$ and $LST_{2004}$, demonstrating significant spatial structure at the maximum distances of 21.2 km and 29.4 km, respectively (Table 3). The proportion of structural variance accounted for 0.500 and 0.501 for $LST_{1997}$ and $LST_{2004}$, with the variability in model strength (as indicated by $r^2$, the coefficient of determination of the semivariogram models) proportional to the structural variance. This implied that random factors might play an important role in determining the spatial heterogeneity of UHI pattern. Therefore, the processes on smaller scales should not be ignored.

In addition, Figs. 8 and 9 show the range or estimated maximum distance at which significant spatial autocorrelation appeared to be somewhat less than that determined by Moran's *I*. However, increase in effective range of semivariogram was in consistent with the scale determined by Moran's *I*. Thus, both the estimated distances indicated the increasing extent and magnitude of UHI over the study period.

*3.4.3. Fractal analysis of UHI patterns*

As indicated in Section 3.4.2, the effective range of semivariograms of LSTs increased remarkably from 21.2 km to 29.4 km, implying that fractals existed on meso scales with the sprawling urban built-up areas. In this study, analysis of the Hausdorff–Besicovitch dimension is based on an analysis of semivariance, therefore, they are both sensitive to the same analysis parameters. The Hausdorff–Besicovitch dimension was used as an alternative to explain the spatial and temporal pattern of UHI in Shanghai. Table 4 shows the statistics of the Hausdorff–Besicovitch dimension ($D$) in all directions, which may reflect the variation of human activities along urban and rural gradient. Significantly, fractal dimension ($D$) of $LST_{1997}$ and $LST_{2004}$ in the direction of E–W (90°) were both much lower than that in the other directions, with the lowest standard errors and the highest coefficient of determination. It can be concluded that in this direction the spatial heterogeneity was mainly associated with structural variance. For $LST_{2004}$, fractal dimension ($D$) in the direction of NE–SW (135°) was slightly higher than that in E–W (90°), with lower standard error and the secondly significant coefficient of determination. In contrast, dimensions and theirs standard errors in other directions were much higher, with lower coefficient of determination. These implied the significant role of random factors and complex patterns of UHI.

## 4. Discussion

Impacts of expansion of urban areas on thermal environment have been well documented. Among the factors causing the UHI effect, canyon geometry, thermal properties of materials, anthro-

**Table 3**
Semivariogram models and parameters of $LST_{1997}$ and $LST_{2004}$.

| Variable | Nugget variance ($C_0$) | Total model variance ($C_0 + C$) | Structural variance ($C/(C_0 + C)$) | Range ($A_0$/km) | $r^2$ | RSS |
|---|---|---|---|---|---|---|
| $LST_{1997}$ | 4.220 | 8.441 | 0.500 | 21.2 | 0.400 | 0.0794 |
| $LST_{2004}$ | 4.220 | 8.450 | 0.501 | 29.4 | 0.241 | 0.221 |

**Table 4**
Fractal dimension features of $LST_{1997}$ and $LST_{2004}$.

| Direction | Fractal dimension | | Standard error | | $r^2$ | |
|---|---|---|---|---|---|---|
| | $LST_{1997}$ | $LST_{2004}$ | $LST_{1997}$ | $LST_{2004}$ | $LST_{1997}$ | $LST_{2004}$ |
| 0° | 1.970 | 1.984 | 0.546 | 1.551 | 0.117 | 0.016 |
| 45° | 1.978 | 1.973 | 0.931 | 1.043 | 0.044 | 0.035 |
| 90° | 1.927 | 1.941 | 0.118 | 0.108 | 0.733 | 0.766 |
| 135° | 1.980 | 1.948 | 0.548 | 0.332 | 0.117 | 0.260 |

pogenic heat, the urban greenhouse effect, and evaporation surfaces may play the important role (Santamoouris, 2002). In respond to removal of the natural land covers and the introduction of artificial materials (e.g., concrete, asphalt, tiles, metals, etc.) dramatically changes radiative, thermal, moisture, roughness and emissivity of the surface and the atmosphere above (Roth, 2002). The resultant alternation of surface energy fluxes occurred, with a consequent increase in the Bowen ratio (the ratio of sensible to latent heat fluxes), which, in turn, causes an increase in temperatures at and above the urban surface (Stull, 1988; Oke, 1982).

Like the other cities in China, previous studies on UHI in Shanghai were typically limited to a finite number of *in situ* temperature observations, which had a long data record but could be available for interpret the long-term impacts of urbanization on the climates on small scale. The difference in air temperatures sampled at 21 urban sites and 10 suburban sites were typically used to examine the UHI. However, due to the rapid urban sprwal and subsequent change in temperatures, only 4 sites at the remote suburban area were available (Ding et al., 2002b). On the other hand, over the past decades, satellite-derived land surface temperature (LST) measurements have been widely applied to evaluate the UHI phenomenon, using thermal infrared data from at-satellite thermal sensors, including NOAA AVHRR, AVHRR, Landsat TM/ETM+, and MODIS. Remotely sensed data has higher spatial distribution but low temporal resolution and a shorter data record (Streutker, 2003). Besides, spatial resolution of images derived from the above sensors varied remarkably. Therefore, the time lag and spatial resolution of at-satellite thermal sensors, among numerous other effects, can make dynamics and patterns of UHI to appear as a complex process.

As pointed out in this study, satellite-derived LSTs were acquired on two dates. Obviously, many factors were neglected but the relationship between land use/cover types and surface temperatures was paid more attention. Both *in situ* data and derived LST should be utilized to reveal the real patterns of UHI and make the studies at different places more comparable in the future researches. Furthermore, though not yet available, establishment of a precise transfer function between LST and the near ground air temperature (Nichol, 1994) can be helpful to identify and understand the dynamics and patterns of UHI on all scales. In addition, for patterns of land use and UHI, spatial dependency and heterogeneity existed on different scales. However, the fractal analysis showed in the direction of E–W, the spatial dependency was mainly associated with structural variance. Relatively weak spatial dependency associated with structural variance also existed in the direction of NE–SW, corresponding well to a previous study by Zhang and Wang (2003).

## 5. Conclusions

The main objective of this study was achieved with the demonstration of the successful coupling of remotely sensed data acquired in 1997 and 2004. With the aid of an integrated GIS/RS-based approach, spatial autocorrelation, semivariance, and fractal analysis were used to quantitatively characterize the patterns of recent UHI in Shanghai. Results revealed that both the extent and magnitude of UHI in Shanghai has undergone a significant increase during 1997 and 2004, with the rapid growth of the urbanized and urbanizing areas.

Significant spatial patterning was present in UHI as indicated by LSTs. Spatial autocorrelation analysis demonstrated that there were both positive–negative–positive autocorrelation for $LST_{1997}$ and $LST_{2004}$. Spatial scales showed that the average size of homogeneous patches dominated with the urbanized and urbanizing areas increased remarkably, so did the extent and magnitude of hot spots. Semivariance analysis demonstrated that the variation that could be attributed to structure accounted for approximately 50% of the variation on the scales. Further, a directional analysis of the Hausdorff–Besicovitch dimension showed that in E–S profile the spatial dependency was mainly associated with structural variance. Relatively weak spatial dependency associated with structural variance also existed in the direction of NE–SW. Results implied both changes in land use and consequent UHI across the two transects or profile should be specially taken into account, though the other transects or profiles are also very important. Moreover, the patterns of UHI (as indicated by LSTs) implied the existence of spatial correlation on the scales, random factors also played the significant role in forming the complexity in patterns of UHI.

In this study, our results showed the ongoing growth of extent and magnitude of UHI on regional scale during an interval of 7 years. With the rapid expansion of the urbanized urbaning landscapes, the heating effect of impervious surfaces increased in proportion. This finding corresponds well with the previous observations (Zhou et al., 2001; Ding et al., 2002b). However, change in the bare lands on both dates and its relation with the land surface temperatures has not been studied in the previous study. According to our result, the newly emerging bare lands along the coastal areas and on the remote islands were well vegetated or developed for fishery, and therefore had the significant cooling effect.

Since 1990, Shanghai has experienced substantial economic growth during the process of shaping a globalizing metropolis with an excellent investment environment and international competition. In respond to the overall arrangement of industries, well-developed satellite towns emerged around the central urban area, they formed the new patterns of urban clusters. During this period, great efforts were made to improve the overall thermal environment in the central urban area, including removing the residences to the satellite towns and rebuild the water bodies and green space in the inner part of the central urban area. It was found that recently the increasing green space can partly help to mitigate the UHI effect in the central urban area (Ding et al., 2002a; Ge et al., 2005). However, at regional level, annual increase in vegetated area was much lower than that of the urbanized and urbanizing area. Therefore, the cooling effect of the vegetation was too limited. It can be expected that the increasing extent of the urbanized and urbanizing area will continue to increase in the foreseeable future, so will the extent and magnitude of UHI. Therefore, policies for controlling and mitigating UHI effect should be taken into account when making the future urban planning.

## Acknowledgements

This study was partly supported by the Youth Science Foundation of Fudan University (Grant No. EXH591330) and Key project of national social science of China (Grant No. 06&ZD024). The authors are grateful to Prof. Bai-lian (Larry) Li's great effort in enhancing the quality of this manuscript.

## References


Anselin, L., 1995. Local indicators of spatial association—LISA. Geographical Analysis 27, 93–115.

Artis, D.A., Carnahan, W.H., 1982. Survey of emissivity variability in thermography of urban areas. Remote Sensing of Environment 12, 313–329.

Burrough, P.A., 1981. Fractal dimensions of landscapes and other environmental data. Nature 294, 240–242.

Carlson, T.N., Augustine, J.A., Boland, F.E., 1977. Potential application of satellite temperature measurements in the analysis of land use over urban areas. Bulletin of the American Meteorological Society 58, 1301–1303.

Carnahan, W.H., Larson, R.C., 1990. An analysis of urban heat sink. Remote Sensing of Environment 33, 65–71.

China National Committee of Agricultural Divisions, 1984. Technical Regulation of Investigation on Land Use Status. Surveying and Mapping Publishing House, Beijing (in Chinese).

Cliff, A.D., Ord, J.K., 1981. Spatial Processes: Models and Applications. Pion, London.

Curran, P.J., Atkinson, P.M., 1998. Geostatistics and remote sensing. Progress in Physical Geography 22, 61–78.

Ding, J.-C., Zhou, H.-M., Ye, Q.-X., 2002a. Importance of city green by investigation on evolution of heat island in Shanghai City. Meteorological Monthly 28 (2), 22–24 (in Chinese).

Ding, J.-C., Zhang, Z.-K., Xi, H., Zhou, H.-M., 2002b. A study of the high temperature and heat island effect in the summer of Shanghai area. Chinese Journal of Atmospheric Sciences 26 (3), 412–420 (in Chinese).

Ge, W.-Q., Zhou, H.-M., Tu, D.-J., 2005. The surveying on thermal influence area of Shanghai urban greenbelt. Remote Sensing Technology and Application 20, 496–500 (in Chinese).

Griffith, D.A., 1987. Saptial Autocorrelation: A Premier. Association of American Geographs, Washington, DC.

Grimm, N.B., Grove, J.M., Pickett, S.T.A., Redman, C.L., 2000. Integrated approaches to long-term studies of urban ecological systems. Bioscience 50 (7), 571–584.

Hung, T., Uchihama, D., Ochi, S., Yasuoka, Y., 2006. Assessment with satellite data of the urban heat island effects in Asian mega cities. International Journal of Applied Earth Observation and Geoinformation 8, 34–48.

Landsberg, H.E., 1981. The Urban Climate. Academic Press, Maryland.

Legendre, P., Legendre, L., 1998. Numerical Ecology. Developments in Environmental Modelling 20. Elsevier, Amsterdam.

Lucas, I.F.J., Frans, J.M., Wel, V.D., 1994. Accuracy assessment of satellite derived land-cover data: a review. Photogrammetric Engineering and Remote Sensing 60, 410–432.

Malaret, E., Bartolucci, L.A., Lozano, D.F., Anuta, P.E., McGillem, C.D., 1985. Landsat-4 and Landsat-5 Thematic Mapper data quality analysis. Photogrammetric Engineering and Remote Sensing 51, 1407–1416.

Markham, B.L., Barker, J.K., 1985. Spectral characteristics of the LANDSAT Thematic Mapper Sensors. International Journal of Remote Sensing 6, 697–716.

Masek, J.G., Lindsay, F.E., Goward, S.N., 2000. Dynamics of urban growth in the Washington DC metropolitan area, 1973–1996, from Landsat observations. International Journal of Remote Sensing 21, 3473–3486.

Masuda, K., Takashima, T., Takayama, Y., 1988. Emissivity of pure and sea waters for the model sea surface in the infrared window region. Remote Sensing of Environment 24, 313–332.

Nichol, J.E., 1994. A GIS-based approach to microclimate monitoring in Singapore's high-rise housing estates. Photogrammetric Engineering and Remote Sensing 60, 1225–1232.

Price, J.C., 1979. Assessment of the urban heat island effect through the use of satellite data. Monthly Weather Review 107, 1554–1557.

Rao, P.K., 1972. Remote sensing of urban "heat islands" from an environmental satellite. Bulletin of the American Meteorological Society 53, 647–648.

Roth, M., 2002. Effects of cities on local climates. In: Proceedings of Workshop of Institute for Global Environment Studies/Asia-Pacific Network (IGES/APN) Mega-city Project. Kitakyushu, Japan (CD-ROM).

Roth, M., Oke, T.R., Emery, W.J., 1989. Satellite-derived urban heat islands from three coastal cities and the utilization of such data in urban climatology. International Journal of Remote Sensing 10, 1699–1720.

Santamoouris, M. (Ed.), 2002. Energy and Climate in the Urban Built Environment. James and James Science Publishers, London.

Shanghai Municipal Statistics Bureau, 2005. Shanghai Statistical Yearbook (2004). China Statistical Press, Beijing (in Chinese with English annotation).

Shen, Z.-W., 1994. Development of Pudong: new pattern of urbanization in China. Shanghai Economic Research 12, 22–24 (in Chinese).

Streutker, D.R., 2003. Satellite-measured growth of the urban heat island of Houston, Taxas. Remote Sensing of Environment 85, 282–289.

Stull, R.B., 1988. An Introduction to Boundary Layer Meterology. Kluwer Academic, Dordrecht.

Tang, Q.-Y., Feng, M.-G., 2002. DPS© Data Processing System for Practical Statistics. Science Press, Beijing (in Chinese).

Voogt, J.A., Oke, T.R., 1998. Effects of urban geometry on remotely-sensed surface temperature. International Journal of Remote Sensing 19, 895–920.

Oke, T.R., 1982. The energetic basis of the urban heat island. Quarterly Journal of the Royal Meteorological Society 108 (455), 1–24.

Weng, Q.-H., Lu, D.-S., Schubring, J., 2004. Estimation of land surface temperature–vegetation abundance relationship for urban heat island studies. Remote Sensing of Environment 89, 467–483.

Xu, H.-Q., Chen, B.-Q., 2004. Remote sensing of the urban heat island and its changes in Xiamen City of SE China. Journal of Environmental Sciences 16, 276–281.

Zhang, C.-S., Zhang, S., He, J.-B., 1998. Spatial distribution characteristics of heavy metals in the sediments of Changjiang river system: spatial autocorrelation and fractal methods. Acta Geographica Sinica 53 (1), 87–96 (in Chinese).

Zhou, H.-M., Zhou, C.-H., Ge, W.-Q., Ding, J.-C., 2001. The surveying on thermal distribution in urban based on GIS and remote sensing. Acta Geographica Sinica 56 (2), 189–197 (in Chinese).

Zhou, S.-Z., Zhang, C., 1985. An Introduction to Urban Climatology. East China Normal University Press, Shanghai (in Chinese).

Zhang, H., Wang, X.-R., 2003. Urban land use/cover dynamics of Shanghai metropolitan area and its potential impact on local air environment. Journal of Fudan University (Natural Science) 42 (6), 925–929 (in Chinese).